# JACS
JOURNAL OF THE AMERICAN CHEMICAL SOCIETY

# Fundamental Insights into the Degradation and Stabilization of Thin Layer Black Phosphorus

Gonzalo Abellán,[†] Stefan Wild,[†] Vicent Lloret,[†] Nils Scheuschner,[‡] Roland Gillen,[‡] Udo Mundloch,[†] Janina Maultzsch,[‡,§] Maria Varela,[∥] Frank Hauke,[†] and Andreas Hirsch*,[†]

[†]Chair of Organic Chemistry II and Joint Institute of Advanced Materials and Processes (ZMP), Friedrich-Alexander-Universität Erlangen-Nürnberg (FAU), Henkestraße 42, 91054 Erlangen, Germany

[‡]Institut für Festkörperphysik, Technische Universität Berlin Hardenbergstrasse 36, 10623 Berlin, Germany

[§]Department of Physics, Chair of Experimental Physics, Friedrich-Alexander-Universität Erlangen-Nürnberg, Erwin-Rommel-Straße 1, 91058 Erlangen, Germany

[∥]Universidad Complutense de Madrid, Instituto Pluridisciplinar, Instituto de Magnetismo Aplicado & Departamento de Física de Materiales, Madrid 28040, Spain

**S** *Supporting Information*

**ABSTRACT:** Herein, we have developed a systematic study on the oxidation and passivation of mechanically exfoliated black phosphorus (BP). We analyzed the strong anisotropic behavior of BP by scanning Raman microscopy providing an accurate method for monitoring the oxidation of BP via statistical Raman spectroscopy. Furthermore, different factors influencing the environmental instability of the BP, i.e., thickness, lateral dimensions or visible light illumination, have been investigated in detail. Finally, we discovered that the degradation of few-layer BP flakes of <10 nm can be suppressed for months by using ionic liquids, paving the way for the development of BP-based technologies.
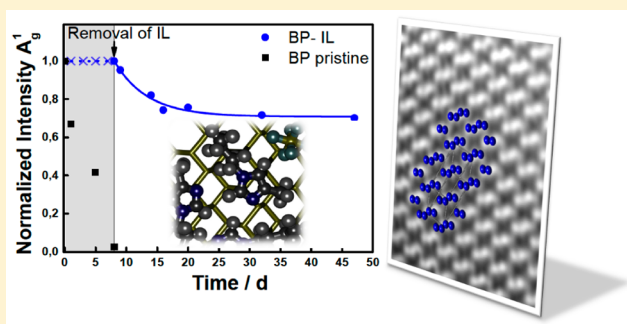
## INTRODUCTION

Black phosphorus (BP) is currently receiving enormous attention as a new 2D material, whose properties in some cases outperform even those of graphene. For example, it exhibits a direct band gap, which spans over a wide range (0.3–2 eV).[1−6] Furthermore, BP exhibits an excellent carrier mobility of up to *ca.* 1000 $cm^2 \cdot V^{-1} \cdot s^{-1}$, a good current on/off ratio (*ca.* $10^4-10^5$), and an exotic in-plane anisotropy that renders this 2D material unique for thermal imaging, thermoelectrics, sensing, fiber optics communication, and photovoltaics, to name only a few (see Figure 1).[2,7−11] However, one major challenge for realizing such exciting applications is to overcome the intrinsic instability of mono- and few-layer nanosheets of BP, which can be obtained by mechanical exfoliation of the bulk crystals[1,8] as well as solvent exfoliation.[12,13] This instability especially against ambient oxygen and moisture leads to a fast oxidative degradation.[14−18] In addition, light irradiation can foster the degradation through photo-oxidation.[15] Although bulk crystals of BP are more stable, thin flakes of BP with smaller than 10 nm thickness degrade in days, whereas single- and few-layer samples may even degrade within hours.[8,16] Different stabilization routes to preserve its intrinsic properties have been developed, including $Al_2O_3$, $TiO_2$, titanium sulfonate ligand ($TiL_4$), polyimide, or aryl diazonium functionalization.[7,19−23] Encapsulation with other 2D materials has also been

explored using graphene or hexagonal boron nitride (*h*BN).[19] Nevertheless, the protection efficiency is still very limited. Recently, it has been reported that high-boiling point solvents like 1-methyl-2-pyrrolidone (NMP) or 1-cyclohexyl-2-pyrrolidone (CHP) are expected to form tightly packed solvation shells in close proximity to the BP surface, acting as a penetration barrier for oxygen.[12,14,17] Similarly, by means of noncovalent functionalization of BP with perylene diimides (PDI), we have recently demonstrated to dramatically increase the stability of few-layer BP.[24] Moreover, as reported by Brent et al., surfactant stabilized FL-BP nanosheets in aqueous media exhibited a slow degradation forming $PO_x$ species and showing a metastable behavior.[25] Although these are promising approaches, an efficient stabilization of BP also compatible with manufacturing of high performance devices remains still an unsolved problem.[4]

The oxidative degradation of BP is a chemical process. After having pioneered the chemical functionalization of graphene,[26−28] we just recently obtained insights on the noncovalent functionalization of BP.[24] We now present a detailed and systematic investigation on the oxidative decomposition of few-layer BP with unprecedented thorough-
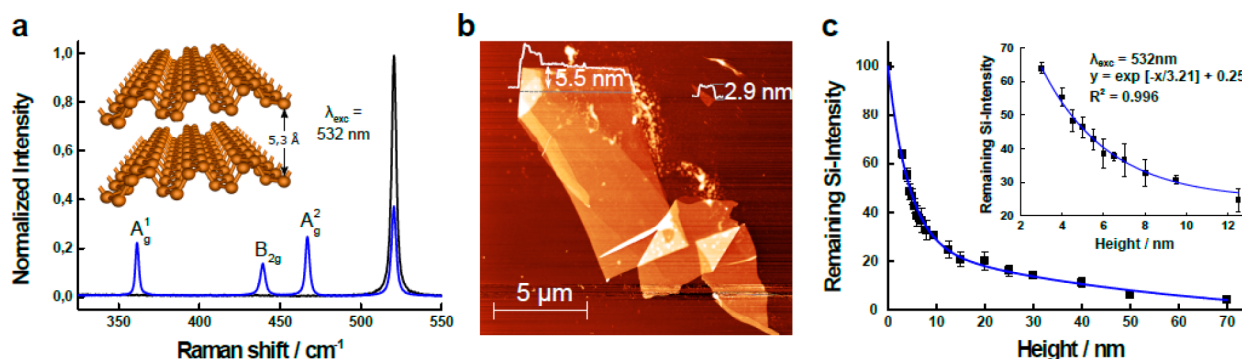
**Figure 1.** (a) Representative Raman spectra of BP (blue) and $SiO_2/Si$ substrates used for this study. The inset shows the chemical structure of BP, highlighting the interlayer distance of 5.3 Å. (b) AFM image of an origami-like BP flake with different terraces and orientations due to its folding. The thinner areas exhibit a thickness of *ca.* 2.9 nm. (c) Normalized silicon intensity attenuation plot (%) measured using different flakes. The inset shows the height below 12 nm. The curve can be adjusted by an exponential decay type I.

ness. Our approach is the combined monitoring of the degradation process using atomic force microscopy (AFM) and Raman spectroscopy, which allowed us to establish easy to use calibration curves. We have also identified a variety of diagnostic fingerprints such as the $A^1_g/A^2_g$ ratio in the Raman spectra, the anisotropy and laser wavelength dependence of Raman spectra, and the influence of flake thickness and its lateral dimensions. For the first time, we also used scanning Raman microscopy (SRM) and statistical Raman spectroscopy (SRS) in order to quantify the decomposition process. In these studies, we discovered elusive Raman signatures of BP, namely the $B_{3g}$- and $B_{1g}$-bands that are due to turbostratic disorder between the layers. We have complemented our results with density functional theory (DFT) calculations. Finally, we analyzed two straightforward passivation routes using commercial solvents like NMP and an imidazolium-based ionic liquid (IL). In particular, we elaborated an unprecedented refinement of BP by IL-passivation in the course of a solvent assisted bulk removal of the IL from the BP flake surface, leaving behind a very thin but highly efficient protection layer. The latter achievement can pave the way for using protected BP films in real world applications.

## ■ RESULTS AND DISCUSSION

For the systematic and quantitative analysis of the decomposition behavior of thin layer BP, we prepared BP nanosheets applying micromechanical exfoliation of BP using a Scotch Tape.[1,8] We have optimized this procedure, which was carried out under the inert conditions of an argon-filled glovebox (<0.1 ppm of $H_2O$ and $O_2$) starting from a finely grinded sample.[15] For the Raman spectroscopy and AFM analysis, the obtained BP flakes were deposited on 300 nm thick $SiO_2/Si$ substrates.

To support our experiments, the phonon frequencies of mono-, bi-, and bulk BP were computed with van der Waals corrected density functional theory (DFT). In particular, we have considered the structural anisotropy of BP that introduces a peculiar dependence of the assignment of the symmetries of the lattice vibrations on the chosen coordinate system.[29,30] To achieve compatibility with the previous reports, an orientation in which the normal of the BP planes is parallel to the *y*-axis, whereas *x* and *z* axes are parallel to the layers, was chosen. As a result, for monolayer and bulk BP three Raman lines in backscattering geometry can be expected: $A^1_g$ at ~355 cm$^{-1}$, $B_{2g}$ at ~434 cm$^{-1}$, and $A^2_g$ at ~460 cm$^{-1}$. In general, multilayer 2D materials can show additional Raman active phonons

compared to bulk and single-layer.[31] This is also the case for BP. We refer to the Supporting Information (SI 1 and 2) for a detailed analysis of the normal modes of multilayer BP, the computed frequencies, and the computational details.

Before we give insights into the analysis of the decomposition process itself, we want to report on a series of fundamental spectroscopic features that we have discovered and analyzed systematically and in detail. These features can serve as a characteristic and diagnostic fingerprint for carefully monitoring both the decomposition and protection of thin BP films. To provide an efficient Raman- and AFM-monitoring of the BP decomposition and its protection, flakes of interest were located by optical microscopy immediately before the Raman or AFM measurements were conducted. We applied statistical Raman spectroscopic analysis as it is a very powerful technique, and it has recently been introduced for the quantitative investigation of the functionalization of graphene and which application is so far unprecedented in BP chemistry.[32,33] The key point in our investigation was to investigate the very pronounced influence of the BP flake morphology, its thickness, and its anisotropy on the oxidative decomposition process. A typical Raman spectrum of BP is presented in Figure 1a. In accordance with previous reports and our DFT calculations, three Raman active modes at frequencies 362, 440, and 466 cm$^{-1}$ can be identified and assigned to $A^1_g$, $B_{2g}$, and $A^2_g$ symmetries, respectively.[30]

One of the main problems of the solely qualitative investigation of the BP degradation, which has been carried out so far, is that it was only based on an AFM investigation, and this technique is quite time-consuming, which makes careful monitoring (including reliable thickness measurements) a very difficult task. Therefore, fast and reliable spectroscopic screening is required to determine the impact and extent of the environmental-based degradation of the BP flakes prior to their subsequent processing. Following this, we systematically studied several flakes of different thicknesses, first by Raman spectroscopy and afterward by AFM (Figure 1b), which allowed us to establish a fundamental calibration curve for the oxidative degradation. As demonstrated in Figure 1c, it turned out that by correlating the normalized remaining Raman silicon intensity at 521 cm$^{-1}$ with the thicknesses determined by AFM over a broad range of samples, it is possible to obtain a robust calibration curve for determining the thickness of a selected BP flake by the application of Raman spectroscopy. Here it is fundamental to keep the acquisition parameters

constant and avoid a prolonged light exposure of the freshly exfoliated flakes (see Experimental Information). The resulting plot (see Figure 1c) can be fitted very accurately by an exponential decay type I. As a first insight, when the remaining Si intensity is above 30% compared to the pure substrate, it can be concluded that the BP flakes under investigation are thinner than 10 nm. It is worth mention that, for most of the applications, monolayer BP is not required, but flakes in the range around 10 nm are of fundamental interest.[3]

With the development of this methodology, we were able to study the Raman features of BP flakes with a controlled thickness in the first stages before degradation occurred. In this line, the anisotropy of BP, which strongly impacts electrical, thermal as well as optical properties, was investigated.[11] As already reported, the intensity of each individual BP Raman mode is highly dependent on the relative angle in which the sample is rotated in the $xz$-plane (incoming laser direction along the $z$-axis).[34] To gain information on the anisotropy, each single BP flake was measured at varying angles by scanning Raman microscopy (SRM) (Figure 2a,c).[24,33] It is worth noting
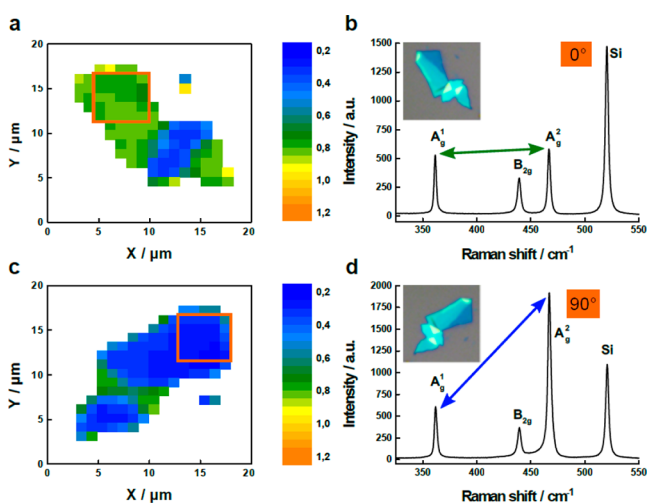


**Figure 2.** (a) SRM analysis of the same flake studied in Figure 1 showing the corresponding $A^1_g/A^2_g$ band ratio mapping measured in the "HRR" (armchair), and (b) its corresponding mean Raman spectra (excitation at 532 nm) of the areas indicated in panel a. The inset is an optical microscopy image of the same flake. (c) SRM analysis of the same flake showing the corresponding $A^1_g/A^2_g$ ratio Raman mapping measured in the "LRR" (zigzag), and (d) its corresponding mean Raman spectra. The arrows highlight the relative differences in the intensities of the $A^1_g$ and $A^2_g$ Raman modes.

that, in general, a step size of 1 $\mu$m in SRM was chosen, as this represents a sufficient resolution and guaranteed relatively fast mappings with reasonable accuracy. Nevertheless, if needed, it is possible to obtain high-resolved BP flakes, located closely next to each other, by reducing the step size to 0.2 $\mu$m (Figure SI3). However, these high-resolution Raman mappings are very time-demanding and normally require more than 20 h of measuring time.

As reported by Martel and co-workers, the $A^1_g/A^2_g$ ratio can be considered as an efficient indicator for the BP degradation.[15] Accordingly, the $A^1_g/A^2_g$ ratio mappings of the origami-like flake shown in Figure 1b were plotted. Our studies clearly indicate that the rotation of the sample in the $xz$-plane by 90° drastically influences the $A^1_g/A^2_g$ ratio, which so far has not been reported. The Raman map obtained at 0° indicates that

the polarization direction of the incident light was parallel to the zigzag crystallographic orientation and along the armchair direction for 90° orientation.[35,36] Here, it has to be mentioned that according to Dresselhaus and co-workers, the maximum BP Raman intensities also strongly depend on the height of flakes upon rotation.[30] Moreover, a precise determination of the crystallographic orientation by means of Raman spectroscopy for a given thickness and excitation wavelength requires further investigations. For flakes with thicknesses below *ca.* 10 nm (like the one presented in this study) and measured using a 532 nm excitation wavelength, the $A_g$ main axis is reported to be along the zigzag crystal orientation (Figure SI4).[30,35,36] For clarity reasons from now on, we will define the high ratio region as "HRR", and the low ratio region as "LRR". Figure 2b,d shows the mean Raman spectra of the selected area (orange), which nicely illustrate the difference in the $A^1_g/A^2_g$ ratio for both orientations, highlighted by the green and blue arrows. Moreover, the $A^2_g$ vibrational Raman mode of BP is the most affected one upon rotation in terms of total intensities, which is in good accordance with recent reports (Figure SI5).[11,34,35] As expected, according to the 2-fold symmetry of BP crystals, further rotation of the sample for 180° results in a similar value of the $A^1_g/A^2_g$ ratio to the one measured at 0° (SI 4 and SI 6). These Raman mappings allow a rapid determination of the orientation of the sample with respect to the polarization of the laser for flakes below *ca.* 10 nm, paving the way for the study of the influence of anisotropy on BP oxidation (*vide infra*).

Furthermore, the influence of the excitation wavelength on the Raman spectra of BP and especially on the $A^1_g/A^2_g$ ratio was evaluated. For this purpose, we exfoliated BP down to a monolayer and measured it along the zigzag direction (LRR) using different excitation wavelengths ranging from 457 to 633 nm. It is important to emphasize that these experiments should be performed in less than 30 min under ambient conditions to avoid the degradation of the flake, which is clearly reflected in the AFM image with the formation of holes and the preferential bubble formation in the edges.[12,24] Figure 3b shows the Raman single point spectra normalized against the $A^2_g$ mode. This plot clearly corroborates a decrease in the $A^1_g$ mode with increasing laser energies. This trend was confirmed for FL-BP as well as for bulk BP and is valid in both orientations. However, for the bulk in the case of the HRR, the $A^1_g/A^2_g$ ratio is not reduced as much as in FL-BP. In comparison, when measuring in the LRR, the intensity of the $A^1_g$ mode substantially diminishes at an excitation wavelength of 457 nm, independently of the thickness (Figure 3b and SI 5). The systematic extinction of the $A^1_g/A^2_g$ ratio for increasing excitation energy might be related to the previously reported anisotropic electron−phonon and electron−photon coupling in BP, which also leads to a different polarization dependence of $A^1_g$ and $A^2_g$ modes.[30]

Moreover, we discovered weakly occurring Raman signals at 195 and 230.5 cm$^{-1}$ for bulk BP (>50 nm). These fit well to two Raman active phonon modes with frequencies at 196 cm$^{-1}$ (symmetry $B_{3g}$) and 235 cm$^{-1}$ (symmetry $B_{1g}$) from our DFT calculations (Supporting Information S1), which should only be detectable in a cross scattering configuration on the grounds of optical selection rules. The appearance of these Raman modes in a backscattering geometry might be attributed to turbostratic disordering of the stacked layers, being related to the presence of edge phonon modes (Figure 3c).[37] The observation of these turbostratic peaks requires long acquisition times.

Equipped with this collection of diagnostic Raman tools, we were in a very good position to quantitatively follow the
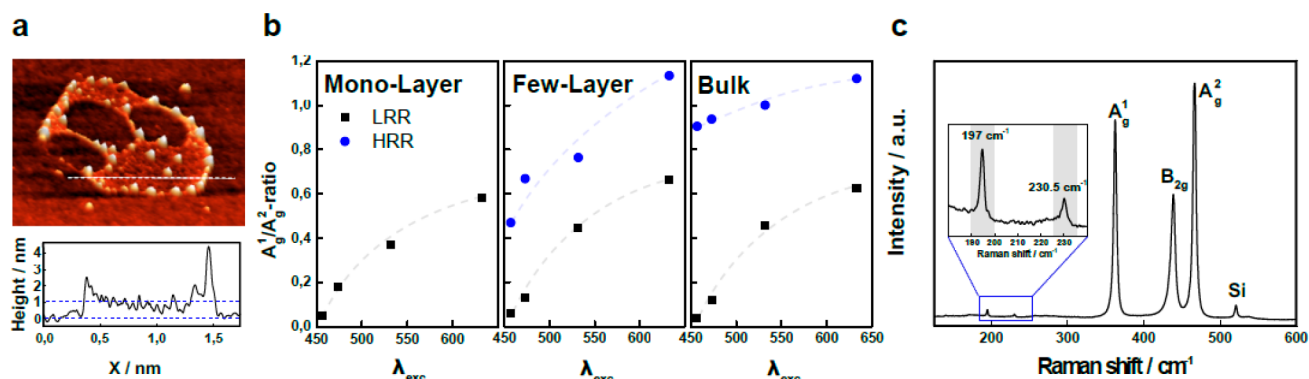
**Figure 3.** (a) Top: Representative AFM image of a monolayer of BP, showing the formation of small droplets and holes due to degradation. Bottom: Height profile showing a thickness of *ca.* 1 nm. (b) Wavelength-dependence $A_g^1/A_g^2$ ratio Raman analysis for a monolayer, few-layers (*ca.* 7 nm), and bulk samples, highlighting the differences between the HRR and LRR. (c) Average Raman mean spectra (532 nm) of a bulk sample after a long acquisition time showing the $B_{3g}$ (196 cm$^{-1}$) and $B_{1g}$ (235 cm$^{-1}$) bands corresponding to the turbostratic disorder between the layers, and the presence of edge phonon modes.

oxidative degradation of few-layer BP at a high level of precision. Therefore, we conducted Raman mappings from several samples over time, measuring every 24 h, using an excitation wavelength of 532 nm and carried out statistics (SI 7). The oxidation process can be monitored both in the HRR and LRR. With ongoing oxidation time, there is a clear evolution in the histograms of the $A_g^1/A_g^2$ ratio toward lower distributions, which becomes more evident after 72 h of environmental degradation (Figure 4a,b). Figure 4c,d shows the mean value extracted from all histograms to easily follow the development of the $A_g^1/A_g^2$ ratio versus time. Our analysis reveals that for both orientations, the characteristic $A_g^1/A_g^2$ ratio decreases. This reflects the usefulness of this methodology for monitoring the oxidation of BP flakes.[12,15,24]

Significantly, this trend can be followed much more easily in the HRR because here the decrease is more pronounced. Therefore, the HRR is more sensitive for monitoring the degradation of BP via SRS. As a consequence from here on, we always selected the HRR orientation for monitoring the oxidation process.

In parallel, AFM images were acquired to follow the oxidation behavior, which is typically reflected in the appearance of droplets. Ziletti and co-workers revealed that the degradation of BP starts with the formation of hydrophilic $P_xO_y$ species after the chemisorption of oxygen, which absorbs water leading to the formation of phosphoric and phosphorus acids.[38] It was also demonstrated that water itself does not oxidize BP as long as it is properly degassed, and that the pristine BP surface is hydrophobic but is turned progressively hydrophilic by oxidation.[39,40] These initially small protuberances evolve with the time until a final coalescence is observed, exhibiting a dramatic increase in the volume (SI 8).[16] However, the influence of thickness and lateral dimensions on the oxidation kinetics remains unclear. Along this line, SRS and AFM studies were performed with samples of different heights in order to identify whether there is any dependence on the thickness. It is worth mention that, in our studies, no evaporated aluminum oxide layers were used to prevent degradation, in contrast to previous reports.[7,22] Indeed, for samples with thicknesses above 10 nm, no decrease of the $A_g^1/A_g^2$ ratio could be observed anymore (SI 9). For this reason, we decided to follow the oxidation measuring the total intensities for each individual BP Raman mode. Figure 4e shows the time dependence of the mean value of the $A_g^1$ vibrational mode,
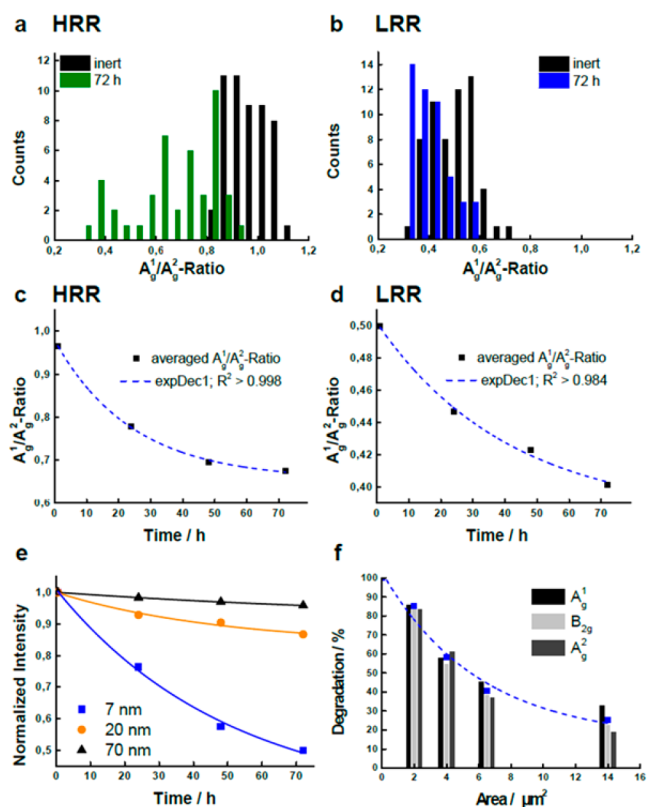


**Figure 4.** (a) Histogram of the $A_g^1/A_g^2$ intensity ratio in the HRR and (b) LRR of pristine BP measured under inert conditions, and after 72 h submitted to environmental conditions. (c) $A_g^1/A_g^2$ intensity ratio evolution with time for the HRR and (d) LRR, showing a typical exponential decay. (e) Influence of thickness in the environmental degradation: The evolution of the normalized $A_g^1$ intensity with time indicates a faster degradation of the flakes below 10 nm. (f) Influence of flake surface area in the environmental degradation: The extent of degradation is less than half for flakes with > *ca.* 7 $\mu m^2$ compared to those of *ca.* 2 $\mu m^2$.

which clearly demonstrates that degradation is enhanced with decreasing thickness of the flakes. In this regard, the FL-BP flake with a height of 7 nm loses approximately 50% of total intensity, whereas the flakes with thicknesses above 20 nm degraded by less than 10%. Correlated graphs displaying the development of the Raman intensity loss of the $B_{2g}$ and $A_g^2$
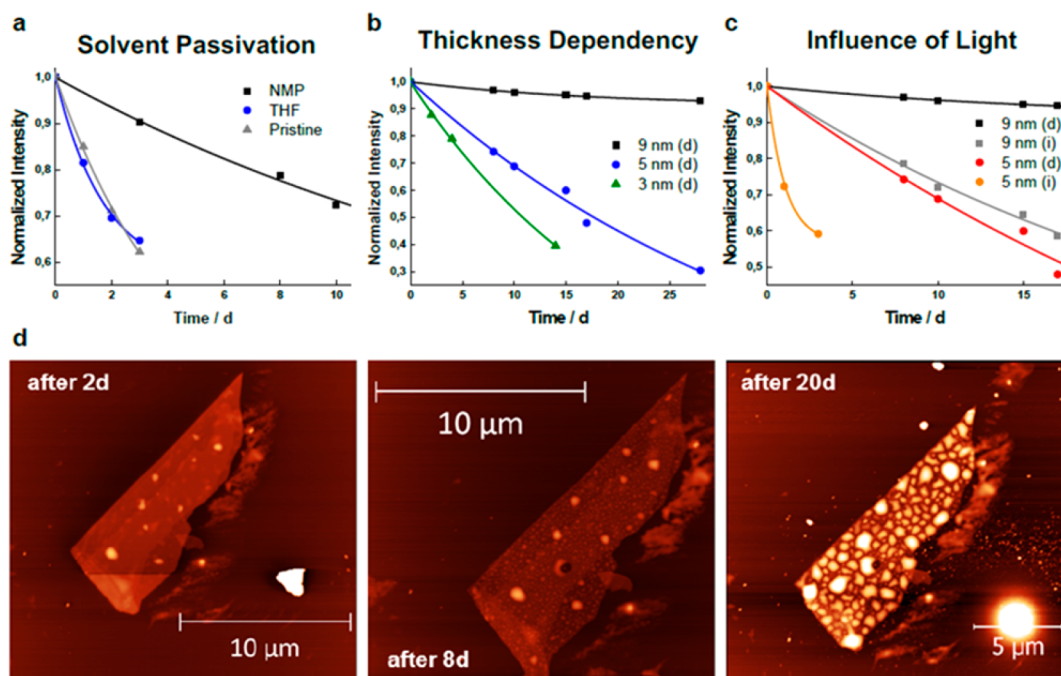
**Figure 5.** (a) Effect of NMP passivation compared to inert solvent (THF) and a pristine sample on *ca.* 5 nm thick flakes with comparable area. (b) Influence of thickness in the degradation of NMP-protected flakes stored in darkness, clearly surpassing 25 days of stability. (c) Influence of continuous visible light illumination on 5 and 9 nm thick flakes. (d) AFM height profile time study of a 9 nm flake protected with NMP after 2, 8, and 20 days under ambient conditions.

modes follow the same trend (SI 10). However, it is important to note that, in the case of the thinnest flakes, there is a difference in the intensity loss of the $A^1_g$ and $A^2_g$ Raman mode of around 12%, which explains why a decrease of the $A^1_g/A^2_g$ ratio could be clearly observed only for FL-BP (<10 nm) samples.

Considering that the BP oxidation follows a "layer-by-layer thinning effect from top down", only the top layers get oxidized, whereas layers underneath a certain number of oxidized layers stay crystalline.[16] We assume that oxidized layers do not contribute to the overall Raman signal meaning that the lowering of the $A^1_g/A^2_g$ ratio has to be related to an additive effect of the $A^1_g$ peak, which is characteristic for the "out-of-plane" vibrational mode and is known to be sensitive toward the thickness of BP sheets below 10 nm.[8] Consequently, for samples thinner than 10 nm, oxidized layers lower the intensity of the $A^1_g$ mode because their relative percentage is significantly higher in FL-BP flakes than in bulk BP, with the assumption that the number of oxidized layers is more or less the same for all BP flakes, irrespective of their height.

Furthermore, the evolution of Raman intensities for pristine BP flakes of comparable thickness (*ca.* 10 nm , SI 11) but different areas were monitored. As depicted in Figure 4f, the lateral dimensions of the flakes exert a dramatic influence. For example, the degradation for a 2 $\mu m^2$ flake proceeds twice as fast as for a 7 $\mu m^2$ flake. After 5 days of monitoring, the degradation versus the lateral dimensions of the flakes follows an exponential decay.

The same behavior was observed for the normalized intensity of the $A^1_g$ mode plotted versus time (SI 12 and 13). These studies clearly demonstrate the importance of establishing well-defined sample criteria, namely, lateral extension, thickness and orientation in order to quantitatively describe the degradation process of BP.

Able to carefully monitor the oxidation of BP, we started out to elaborate robust concepts for the passivation and protection of thin BP films. Since 2014, several routes have been proposed in order to avoid BP degradation; most of them are focused on preventing its exposure to atmospheric conditions using physical encapsulation with other 2D materials or evaporating metal oxide layers on top of the flakes.[7,19,41] A more straightforward approach is the use of high-boiling point solvents based on pyrrolidones like *N*-methyl-2-pyrrolidone (NMP) or 1-cyclohexyl-2-pyrrolidone (CHP), which can significantly improve the stability of BP to *ca.* 8 days.[12,14,18] To illustrate this passivation effect, we have developed a direct comparison between NMP and THF treated BP thin flakes with identical thickness and comparable area. THF can be considered as an inert solvent toward BP.[24] In fact, degradation of samples treated with THF is identical to pristine ones (Figure 5a).

It can be seen that NMP-protected flakes exhibit much longer lifetimes when monitoring the total Raman intensities. In the course of our stability investigation, we discovered that also NMP-passivated BP flakes reveal pronounced thickness dependent oxidation kinetics. Thicker flakes are even more stable after NMP protection than thinner ones (Figure 5b).

Also, light exposure plays a critical role in the degradation of BP. To demonstrate this, we monitored BP flakes submitted to constant illumination (150 W halogen lamp) by SRS, SRM, and AFM. We found that storing NMP-protected BP flakes in the dark dramatically increases the lifetime, in contrast to samples that were constantly illuminated. Indeed, samples with thicknesses below 10 nm can survive up to 30 days under ambient conditions when stored in the dark (Figure 5c). The corresponding AFM images show that the formation of phosphoric acid (and the water absorption) on the surface of the flakes is much slower for the samples stored in darkness (SI
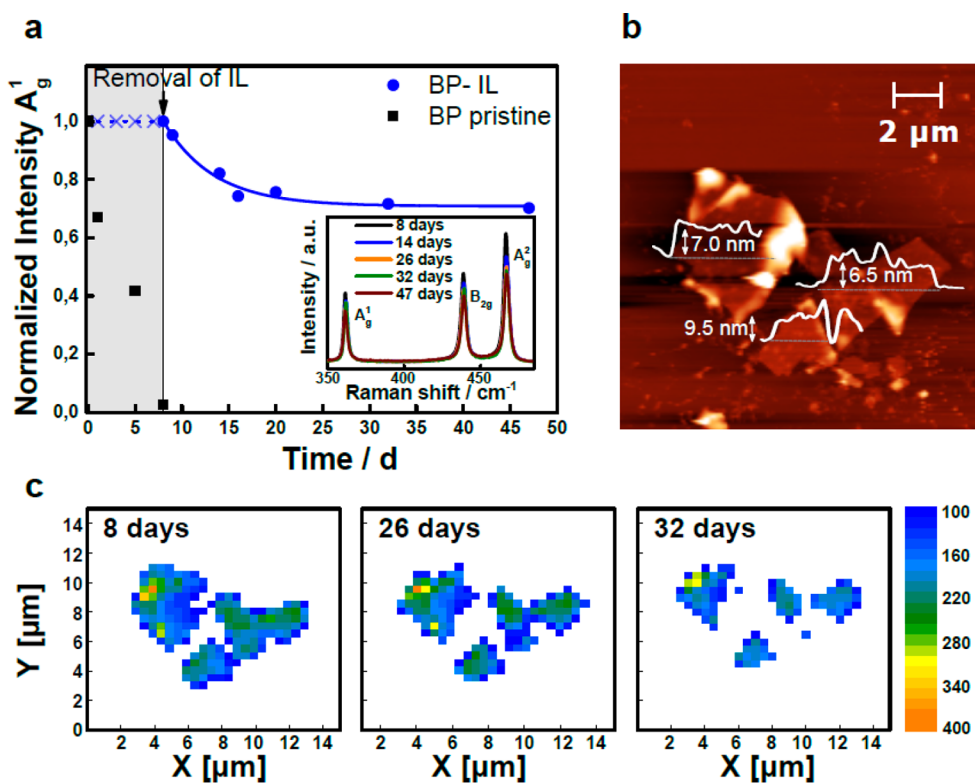
**Figure 6.** Ionic liquid passivation. (a) Evolution of the $A^1_g$ intensities with time, highlighting the outstanding stability of IL-protected flakes. The samples remain stable when covered by BMIM-BF$_4$ droplets, whereas pristine, unprotected BP flakes with similar thicknesses and lateral dimensions completely disappear after *ca.* 7 days. After 7 days, removal of the IL covering by washing leads to intact flakes with no signs of degradation, exhibiting the same initial $A^1_g$ intensity value. The stability study reveals a life of more than 40 days. (b) AFM topography image of cleaned flakes after removing the IL coverage, showing thicknesses between 6 and 10 nm. (c) SRM of the same flakes as in panel b highlighting the evolution of the $A^1_g$ intensities after 8, 26, and 32 days of removal of the IL.

14). This is very important for practical uses, as it opens up the possibility of transporting and manipulating the samples over weeks with a minimum degradation if the storage conditions are adequate.

Although quite successful, the passivation of the flakes with high-boiling point solvents turns out to be problematic for the fabrication of electrical contacts in nanodevices. In this sense, a protective layer with the ability to be easily removed is highly desired. Ionic liquids (IL) are a very promising option, as they have been successfully used as gate dielectrics for BP electric-double-layer transistors (EDLT).[42] Moreover, Zhao and co-workers have already reported that highly concentrated dispersions of BP which are stable during one month can be obtained by sonication in different ionic liquids (IL).[43] In this line, we used 1-butyl-3-methylimidazolium tetrafluoroborate (BMIM-BF$_4$), a commercial environmentally friendly IL that is very stable, exhibits a polar character and high viscosity. The first attempts showed an impressive degradation resistance over weeks without a significant decrease in the Raman intensities, clearly surpassing the performance of the NMP protected flakes.

The passivation studies of BP with ILs so far have always been carried out on the basis of a bulk coverage.[43,44] Here, we report for the first time on a very thin coverage with ILs, which makes this technology highly attractive for practical applications. For this purpose, a comparative study with selected flakes having similar thicknesses and areas (5−10 nm; 2−7 $\mu m^2$) was developed. As shown in Figure 6, a drop of BMIM-BF$_4$ was deposited on the substrates. The substrates were subsequently washed with acetonitrile and isopropyl alcohol in a spin coater to remove the excess of ILs and leave behind a very tightly bound film. The degradation was monitored by SRM.

The pristine flakes without ILs survived for about 7 days, whereas those covered by a thin layer of ILs exhibited an impressive stability. The removal of the ILs after 7 days presents a negligible decrease in the Raman bands of less than 5%. This means that BP flakes can be stored in ionic liquids without degradation, indeed the samples immersed in the IL without the washing procedure remain completely stable for months, allowing an easy transport without taking care of the environmental conditions. As can be seen in Figure 6a, the average normalized intensity evolution of the Raman spectra with time exhibits a decrease of *ca.* 30% after 47 days. This degradation is mainly attributed to the continuous laser exposure for measuring the SRM over time (each Raman mapping last around 30 min). As evidenced by AFM (Figure 6b), only minor residues are left on the surface of the BP flakes. With this experiment, we demonstrated that the passivation with ILs results in an efficient protection of the BP that can be partly reversed by simply washing with an appropriate solvent, which is compatible with the development of (opto)electronical devices.

To gain further insights, on both chemistry and structure, we analyzed an IL-BP sample stored under ambient conditions after 58 days of its preparation by atomic-resolution aberration-corrected scanning transmission electron microscopy (STEM) − electron energy-loss spectroscopy (EELS) at 80 kV (see Supporting Information for additional experimental details).
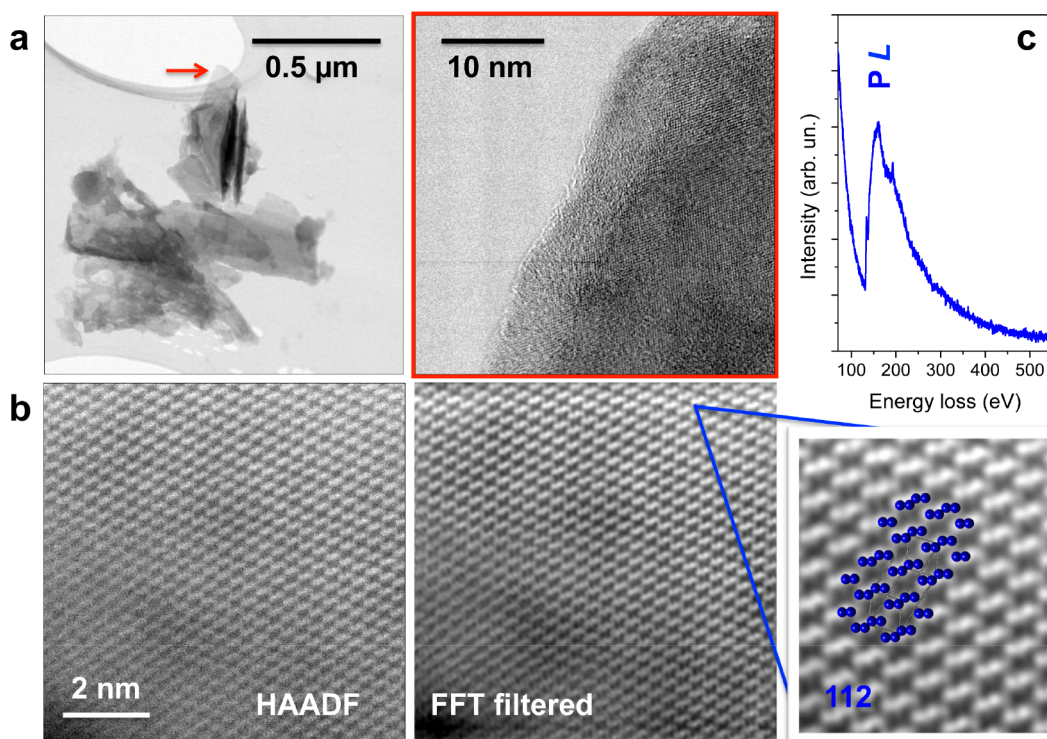
**Figure 7.** STEM-EELS analysis. (a) Low magnification (left) and high magnification (right) ABF images of the flakes. The high magnification image was acquired on the edge of a free-standing portion of a flake (area marked with a red arrow on the left). (b) Atomic resolution HAADF image (left), along with a Fourier filtered (FFT, middle) and a magnified view (right end), acquired down the [112] orientation. A sketch of the structure down this axis is overlaid on the left image (to scale), P atoms shown in blue. (c) EEL spectrum acquired on the free-standing portion of the flake, exhibiting no hints of major C or O signals (within experimental noise). Data acquired at 80 kV.

The suspended IL-BP samples were dropped onto lacey carbon coated copper TEM grids under environmental conditions and washed with ethanol before drying. Moreover, we measured it after submitting the TEM grid to an ambient plasma treatment during 5 min prior to the insertion in the microscope. Low magnification annular bright field (ABF) images exhibit a flake morphology consistent with AFM images (Figure 7a, left). Usually, after a few hours of degradation, pristine BP samples exhibit highly degraded rims, amorphous edges, and the presence of holes.[24] In contrast, the atomic-resolution ABF images, the image in Figure 7a (right) shows a highly crystalline BP flake with a very minor degree of amorphization on the edges and step-like morphology near the edges after 58 days of preparation and storage under environmental conditions. Atomic resolution high-angle annular dark field (HAADF) images were acquired down the [112] crystallographic axis. Figure 7b exhibits a raw HAADF image (left) along with a Fourier filtered image (middle) and a magnified view with a sketch of the crystal structure overlaid (right). The flakes are crystalline over long lateral distances of the order of tenths of a micrometer. We also analyzed the chemical composition of the flakes by EELS. Figure 7c depicts an average spectrum measured on the middle of a portion of a flake standing on vacuum (see area marked with a red arrow on Figure 7a). The P $L_{2,3}$-edge is clearly visible, with an onset near 132 eV. No traces of the C K-edge or the O K-edge were observed (near 284, and 532 eV, respectively), thus revealing the impressive resilience of the IL-passivated flakes. The outstanding stability of the IL-BP flakes is attributed to the high surface tension of IL, the Coulombic forces, the amphiphilic interactions, and/or the $\pi-\pi$ interactions given between the positive aromatic cores

of the BMIM-BF$_4$ and BP, creating a compact passivation layer on the surfaces of the BP nanosheets, and precluding the oxygen and water penetration.[24,45,46] Moreover, the imidazoles are excellent candidates for the entrapment and neutralization of reactive intermediate superoxide anions $O_2(aq)^{\bullet-}$,[15,47] and recent biochemical assays have demonstrated that imidazole IL can sequestrate very efficiently several reactive oxygen species,[48] thus minimizing the impact of photo-oxidation in BP flakes.

## ■ CONCLUSION

In summary, we have developed a systematic study on the oxidation and passivation of mechanically exfoliated black phosphorus. By combining AFM, SRM, and SRS, we provided a rapid and reliable methodology to precisely estimate the thickness of BP flakes using the Si-attenuation intensity. Moreover, we highlighted the strong influence of the anisotropy of BP on the $A^1_g/A^2_g$ ratio, which is indicative of the oxidation status. Additionally, we elucidated the dependency of the BP Raman modes with the excitation wavelength, complementing these results with DFT calculations. Furthermore, the influence of thickness and lateral dimensions on the BP oxidation kinetics was clarified. The role of visible light in the photo-oxidation of BP was studied in NMP-protected <10 nm thick flakes, reaching stabilities of 1 month by keeping the samples in darkness.

Finally, we proved that the diffusion of oxygen and water as well as the BP photo-oxidation can be suppressed by covering the flakes with BMIM-BF$_4$ ionic liquid, exhibiting an outstanding stability for months under environmental conditions. This work paves the way for the development of BP chemistry

and provides an effective and partly reversible passivation route compatible with the development of (opto)electronic devices.

## ASSOCIATED CONTENT

**Ⓢ Supporting Information**

The Supporting Information is available free of charge on the ACS Publications website at DOI: 10.1021/jacs.7b04971.

Experimental details, DFT calculations, additional Raman and AFM characterization (PDF)

## AUTHOR INFORMATION

**Corresponding Author**

*andreas.hirsch@fau.de

**ORCID**

Gonzalo Abellán: 0000-0003-1564-6210

Frank Hauke: 0000-0001-9637-7299

**Notes**

The authors declare no competing financial interest.

## ACKNOWLEDGMENTS

## REFERENCES

(1) Liu, H.; Neal, A. T.; Zhu, Z.; Luo, Z.; Xu, X.; Tománek, D.; Ye, P. D. *ACS Nano* **2014**, *8* (4), 4033.

(2) Li, L.; Yu, Y.; Ye, G. J.; Ge, Q.; Ou, X.; Wu, H.; Feng, D.; Chen, X. H.; Zhang, Y. *Nat. Nanotechnol.* **2014**, *9* (5), 372.

(3) Ling, X.; Wang, H.; Huang, S.; Xia, F.; Dresselhaus, M. S. *Proc. Natl. Acad. Sci. U. S. A.* **2015**, *112* (15), 4523.

(4) Castellanos-Gomez, A. *J. Phys. Chem. Lett.* **2015**, *6* (21), 4280.

(5) Rahman, M. Z.; Kwong, C. W.; Davey, K.; Qiao, S. Z. *Energy Environ. Sci.* **2016**, *9* (3), 709.

(6) Gusmao, R.; Sofer, Z.; Pumera, M. *Angew. Chem., Int. Ed.* **2017**, *56*, 8052.

(7) Wood, J. D.; Wells, S. A.; Jariwala, D.; Chen, K.-S.; Cho, E.; Sangwan, V. K.; Liu, X.; Lauhon, L. J.; Marks, T. J.; Hersam, M. C. *Nano Lett.* **2014**, *14* (12), 6964.

(8) Castellanos-Gomez, A.; Vicarelli, L.; Prada, E.; Island, J. O.; Narasimha-Acharya, K. L.; Blanter, S. I.; Groenendijk, D. J.; Buscema, M.; Steele, G. A.; Alvarez, J. V.; Zandbergen, H. W.; Palacios, J. J.; van der Zant, H. S. J. *2D Mater.* **2014**, *1* (2), 25001.

(9) Buscema, M.; Groenendijk, D. J.; Steele, G. A.; van der Zant, H. S. J.; Castellanos-Gomez, A. *Nat. Commun.* **2014**, *5*, 4651.

(10) Qiao, J.; Kong, X.; Hu, Z.-X.; Yang, F.; Ji, W. *Nat. Commun.* **2014**, *5*, 4475.

(11) Xia, F.; Wang, H.; Jia, Y. *Nat. Commun.* **2014**, *5*, 4458.

(12) Hanlon, D.; Backes, C.; Doherty, E.; Cucinotta, C. S.; Berner, N. C.; Boland, C.; Lee, K.; Harvey, A.; Lynch, P.; Gholamvand, Z.; Zhang, S.; Wang, K.; Moynihan, G.; Pokle, A.; Ramasse, Q. M.; McEvoy, N.; Blau, W. J.; Wang, J.; Abellán, G.; Hauke, F.; Hirsch, A.; Sanvito, S.; O'Regan, D. D.; Duesberg, G. S.; Nicolosi, V.; Coleman, J. N. *Nat. Commun.* **2015**, *6*, 8563.

(13) Lewis, E. A.; Brent, J. R.; Derby, B.; Haigh, S. J.; Lewis, D. J. *Chem. Commun.* **2017**, *53*, 1445.

(14) Kang, J.; Wood, J. D.; Wells, S. A.; Lee, J.-H.; Liu, X.; Chen, K.-S.; Hersam, M. C. *ACS Nano* **2015**, *9* (4), 3596.

(15) Favron, A.; Gaufrès, E.; Fossard, F.; Phaneuf-L'Heureux, A.-L.; Tang, N. Y.-W.; Lévesque, P. L.; Loiseau, A.; Leonelli, R.; Francoeur, S.; Martel, R. *Nat. Mater.* **2015**, *14* (8), 826.

(16) Island, J. O.; Steele, G. A.; van der Zant, H. S. J.; Castellanos-Gomez, A. *2D Mater.* **2015**, *2* (1), 11002.

(17) Yasaei, P.; Kumar, B.; Foroozan, T.; Wang, C.; Asadi, M.; Tuschel, D.; Indacochea, J. E.; Klie, R. F.; Salehi-Khojin, A. *Adv. Mater.* **2015**, *27* (11), 1887.

(18) Woomer, A. H.; Farnsworth, T. W.; Hu, J.; Wells, R. A.; Donley, C. L.; Warren, S. C. *ACS Nano* **2015**, *9* (9), 8869.

(19) Doganov, R. A.; O'Farrell, E. C. T.; Koenig, S. P.; Yeo, Y.; Ziletti, A.; Carvalho, A.; Campbell, D. K.; Coker, D. F.; Watanabe, K.; Taniguchi, T.; Neto, A. H. C.; Özyilmaz, B. *Nat. Commun.* **2015**, *6*, 6647.

(20) Lee, H. U.; Lee, S. C.; Won, J.; Son, B.-C.; Choi, S.; Kim, Y.; Park, S. Y.; Kim, H.-S.; Lee, Y.-C.; Lee, J. *Sci. Rep.* **2015**, *5*, 8691.

(21) Zhu, W.; Yogeesh, M. N.; Yang, S.; Aldave, S. H.; Kim, J.-S.; Sonde, S.; Tao, L.; Lu, N.; Akinwande, D. *Nano Lett.* **2015**, *15* (3), 1883.

(22) Ryder, C. R.; Wood, J. D.; Wells, S. A.; Yang, Y.; Jariwala, D.; Marks, T. J.; Schatz, G. C.; Hersam, M. C. *Nat. Chem.* **2016**, *8* (6), 597.

(23) Zhao, Y.; Wang, H.; Huang, H.; Xiao, Q.; Xu, Y.; Guo, Z.; Xie, H.; Shao, J.; Sun, Z.; Han, W.; Yu, X.-F.; Li, P.; Chu, P. K. *Angew. Chem., Int. Ed.* **2016**, *55* (16), 5003.

(24) Abellán, G.; Lloret, V.; Mundloch, U.; Marcia, M.; Neiss, C.; Görling, A.; Varela, M.; Hauke, F.; Hirsch, A. *Angew. Chem., Int. Ed.* **2016**, *55* (47), 14557.

(25) Brent, J. R.; Ganguli, A.K.; Kumar, V.; Lewis, D. J.; McNaughter, P. D.; O'Brien, P.; Sabherwal, P.; Tedstone, A. A. *RSC Adv.* **2016**, *6* (90), 86955.

(26) Englert, J. M.; Dotzer, C.; Yang, G.; Schmid, M.; Papp, C.; Gottfried, J. M.; Steinrück, H.-P.; Spiecker, E.; Hauke, F.; Hirsch, A. *Nat. Chem.* **2011**, *3* (4), 279.

(27) Hirsch, A.; Englert, J. M.; Hauke, F. *Acc. Chem. Res.* **2013**, *46* (1), 87.

(28) Abellán, G.; Schirowski, M.; Edelthalhammer, K. F.; Fickert, M.; Werbach, K.; Peterlik, H.; Hauke, F.; Hirsch, A. *J. Am. Chem. Soc.* **2017**, *139* (14), 5175.

(29) Ling, X.; Liang, L.; Huang, S.; Puretzky, A. A.; Geohegan, D. B.; Sumpter, B. G.; Kong, J.; Meunier, V.; Dresselhaus, M. S. *Nano Lett.* **2015**, *15* (6), 4080.

(30) Ling, X.; Huang, S.; Hasdeo, E. H.; Liang, L.; Parkin, W. M.; Tatsumi, Y.; Nugraha, A. R. T.; Puretzky, A. A.; Das, P. M.; Sumpter, B. G.; Geohegan, D. B.; Kong, J.; Saito, R.; Drndic, M.; Meunier, V.; Dresselhaus, M. S. *Nano Lett.* **2016**, *16* (4), 2260.

(31) Scheuschner, N.; Gillen, R.; Staiger, M.; Maultzsch, J. *Phys. Rev. B: Condens. Matter Mater. Phys.* **2015**, *91* (23), 235409.

(32) Hof, F.; Bosch, S.; Englert, J. M.; Hauke, F.; Hirsch, A. *Angew. Chem., Int. Ed.* **2012**, *51* (47), 11727.

(33) Englert, J. M.; Vecera, P.; Knirsch, K. C.; Schäfer, R. A.; Hauke, F.; Hirsch, A. *ACS Nano* **2013**, *7* (6), 5472.

(34) Zhang, S.; Yang, J.; Xu, R.; Wang, F.; Li, W.; Ghufran, M.; Zhang, Y.-W.; Yu, Z.; Zhang, G.; Qin, Q.; Lu, Y. *ACS Nano* **2014**, *8* (9), 9590.

(35) Lu, W.; Ma, X.; Fei, Z.; Zhou, J.; Zhang, Z.; Jin, C.; Zhang, Z. *Appl. Phys. Lett.* **2015**, *107* (2), 21906.

(36) Kim, J.; Lee, J.-U.; Lee, J.; Park, H. J.; Lee, Z.; Lee, C.; Cheong, H. *Nanoscale* **2015**, *7* (44), 18708.

(37) Ribeiro, H. B.; Villegas, C. E. P.; Bahamon, D. A.; Muraca, D.; Castro Neto, A. H.; de Souza, E. A. T.; Rocha, A. R.; Pimenta, M. A.; de Matos, C. J. S. *Nat. Commun.* **2016**, *7*, 12191.

(38) Ziletti, A.; Carvalho, A.; Campbell, D. K.; Coker, D. F.; Castro Neto, A. H. *Phys. Rev. Lett.* **2015**, *114* (4), 46801.

(39) Huang, Y.; Qiao, J.; He, K.; Bliznakov, S.; Sutter, E.; Chen, X.; Luo, D.; Meng, F.; Su, D.; Decker, J.; Ji, W.; Ruoff, R. S.; Sutter, P. *Chem. Mater.* **2016**, *28* (22), 8330.

(40) Walia, S.; Sabri, Y.; Ahmed, T.; Field, M. R.; Ramanathan, R.; Arash, A.; Bhargava, S. K.; Sriram, S.; Bhaskaran, M.; Bansal, V.; Balendhran, S. *2D Mater.* **2017**, *4* (1), 15025.

(41) Sun, J.; Lee, H.-W.; Pasta, M.; Yuan, H.; Zheng, G.; Sun, Y.; Li, Y.; Cui, Y. *Nat. Nanotechnol.* **2015**, *10* (11), 980.

(42) Saito, Y.; Iwasa, Y. *ACS Nano* **2015**, *9* (3), 3192.

(43) Zhao, W.; Xue, Z.; Wang, J.; Jiang, J.; Zhao, X.; Mu, T. *ACS Appl. Mater. Interfaces* **2015**, *7* (50), 27608.

(44) Lee, M.; Roy, A. K.; Jo, S.; Choi, Y.; Chae, A.; Kim, B.; Park, S. Y.; In, I. *Nanotechnology* **2017**, *28* (12), 125603.

(45) Zhao, Y.; Zhou, Q.; Li, Q.; Yao, X.; Wang, J. *Adv. Mater.* **2017**, *29* (6), 1603990.

(46) Chaban, V. V.; Fileti, E. E.; Prezhdo, O. V. *ACS Nano* **2017**, *11* (6), 6459.

(47) Zhao, L.; Zhang, C.; Zhuo, L.; Zhang, Y.; Ying, J. Y. *J. Am. Chem. Soc.* **2008**, *130* (38), 12586.

(48) Walia, S.; Balendhran, S.; Ahmed, T.; Singh, M.; El-Badawi, C.; Brennan, M. D.; Weerathunge, P.; Karim, M. N.; Rahman, F.; Rassell, A.; Duckworth, J.; Ramanathan, R.; Collis, G. E.; Lobo, C. J.; Toth, M.; Kotsakidis, J. C.; Weber, B.; Fuhrer, M.; Dominguez-Vera, J. M.; Spencer, M. J. S.; Aharonovich, I.; Sriram, S.; Bhaskaran, M.; Bansal, V. *Adv. Mater.* **2017**, 1700152.